IEEE Access
Multidisciplinary | Rapid Review | Open Access Journal

Date of publication xxxx 00, 0000, date of current version xxxx 00, 0000.

*Digital Object Identifier 10.1109/ACCESS.2019.DOI*

# A Unified Framework for HS-UAV NOMA Networks: Performance Analysis and Location Optimization

**XINGWANG LI[1], (Member, IEEE), QUNSHU WANG[1], (Student Member, IEEE), HONGXING PENG[1], HUI ZHANG[2], DINH-THUAN DO[3], (Member, IEEE), KHALED M. RABIE[4], (Member, IEEE), RUPAK KHAREL[5], (Senior Member, IEEE), and CHARLES C. CAVALCANTE[6], (Senior Member, IEEE)**

[1]School of Physics and Electronic Information Engineering, Henan Polytechnic University, Jiaozuo, 454003 China
[2]School of Energy Science and Engineering, Henan Polytechnic University, Jiaozuo, 454003, China
[3]Wireless Communications Research Group, Faculty of Electrical and Electronics Engineering, Ton Duc Thang University, Viet Nam
[4]Department of Engineering, Manchester Metropolitan University, Manchester M1 5GD, U.K.
[5]Department of Computing and Mathematics, Manchester Metropolitan University, Manchester M15 6BH, U.K.
[6]Wireless Telecommunications Research Group, Federal University of Ceara, Campus do Pici, Bl. 722, 60455-760 Fortaleza-CE, Brazil

Corresponding author: Hui Zhang (e-mail:caikuangzhang@163.com.).

**ABSTRACT** In this paper, we propose a unified framework for hybrid satellite/unmanned aerial vehicle (HS-UAV) terrestrial non-orthogonal multiple access (NOMA) networks, where satellite aims to communicate with ground users with the aid of a decode-forward (DF) UAV relay by using NOMA protocol. All users are randomly deployed to follow a homogeneous Poisson point process (PPP), which is modeled by the stochastic geometry approach. To reap the benefits of satellite and UAV, the links of both satellite-to-UAV and UAV-to-ground user are assumed to experience Rician fading. More practically, we assume that perfect channel state information (CSI) is infeasible at the receiver, as well as the distance-determined path-loss. To characterize the performance of the proposed framework, we derive analytical approximate closed-form expressions of the outage probability (OP) for the far user and the near user under the condition of imperfect CSI. Also, the system throughput under delay-limited transmission mode is evaluated and discussed. In order to obtain more insights, the asymptotic behavior is explored in the high signal-to-noise ratio (SNR) region and the diversity orders are obtained and discussed. To further improve the system performance, based on the derived approximations, we optimize the location of the UAV to maximize the sum rate by minimizing the average distance between the UAV and users. The simulated numerical results show that: *i*) there are error floors for the far and the near users due to the channel estimation error; *ii*) the outage probability decreases as the Rician factor $K$ increasing, and *iii*) the outage performance and system throughput performance can be further improved considerably by carefully selecting the location of the UAV.

**INDEX TERMS** Non-orthogonal multiple access (NOMA), unmanned aerial vehicle (UAV), satellite communication, location optimization, Rician fading channels

## I. INTRODUCTION

### A. BACKGROUND

WITH the developments of mobile internet networks (MIN) and internet-of-things (IoT), there are great challenges for the fifth generation (5G) wireless communication to support massive connectivity and seamless connection under limited spectrum. To solve the above problems, a myriad of physical layer technologies have been proposed, such as massive multiple-input multiple-output (MIMO) [1, 2], non-orthogonal multiple access (NOMA) [3, 4], millimeter wave (mmWave) [5, 6], small cell networks (SCNs) [7, 8], satellite communication [9, 10] and unmanned aerial vehicles (UAVs) [11, 12]. Among the above technologies, satellite communication and UAV communication are critical segments to support some applications of the upcoming 5G and beyond networks. The satellite communication has become a promising approach due to the growing demand for higher link reliability, greater capability and wider coverage of wireless services.

Unfortunately, owing to the constrained orbital property and latency, some time-critical and locally enhancing sensing applications are very difficult and even infeasible for satellite only. As supplementary, UAV communication has attracted considerable research interests from academic and industry because of its flexibility, higher maneuverability, low-latency and ease of deployment. Therefore, the hybrid satellite/UAV (HS-UAV) communication is important for further applications, such as precision agriculture, disaster response, prehospital emergency care and mineral exploration,among others [13].

On a parallel avenue, non-orthogonal multiple access (NOMA) is another promising technology to improve spectrum efficiency, enhance massive connections and maintain user fairness [14, 15]. Contrary to the conventional orthogonal multiple access (OMA), NOMA can allow all served users to access the same frequency/code resource at the same time, which can be achieved by power multiplexing.[1] In NOMA, all signals are superimposed and sent simultaneously from the transmitter. At the receiver, the individual signal can be obtained by using successive interference cancellation (SIC). Apart from the above benefits, NOMA can also ensure fairness by allocating more power to the far user and few power to the near user. In light of this fact, there are some literature to focus on the contribution of NOMA, see [16–18] and there references therein. Regarding cellular downlink NOMA systems, authors of [16] derived analytical expressions for the outage probability (OP) and ergodic sum rate over Rayleigh fading channels. Exploiting statistical channel state information (CSI), an optimal power allocation strategy was designed by using max-min fairness criterion [17]. In [18], authors investigated the reliability and security performance of the downlink NOMA networks in the presence of in-phase and quadrature-phase imbalance (IQI).

In order to obtain more diversity gain and enlarge the coverage of the network, cooperative communication has been introduced into NOMA to help the communication between the source and the destinations, which has sparked a great deal of research interests, e.g., see [19–24] and the references therein. In [19], Ding et al. proposed a new cooperative NOMA scheme, where the near user acts as a decode-and-forward (DF) relay to aid the far user under the assumption of the direct link between the base station and the far user. As an important strategy for 5G, Kim et al. extended NOMA into coordinated directly and relay transmission in [20]. Considering the effects of residual hardware impairments on transceivers, Li et al. proposed a novel cooperative simultaneous wireless information and power transfer NOMA (SWIPT-NOMA) protocol and derived the analytical expressions for the outage probability and system throughput [21]. In addition, Lee et al. in [22] designed a partial relay selection of amplify-and-forward (AF) NOMA networks and investigated the effect of the proposed scheme on the outage probability and sum rate. Regarding a full-duplex (FD) scenario, Liu et al. in [23] derived the analytical closed-form expressions for the outage probability and the ergodic sum rate of cooperative NOMA network, where both perfect and imperfect SIC are taken into account. Do et al. in [24] considered the underlay cognitive radio inspired hybrid OMA/NOMA networks, and the outage probability and system throughput of the downlink in the secondary network were investigated and evaluated.

[1]In general, NOMA can be classified into two categories, such as power-domain NOMA and code-domain NOMA. This paper focuses on power-domain NOMA and we use NOMA instead.

### B. MOTIVATIONS AND CONTRIBUTION

Motivated by the aforementioned discussion, in this study, we elaborate on the performance of the HS-UAV networks, where the satellite aims to communicate with NOMA users with the aid of a UAV. To exploit the inherited flexibility of the satellite and UAV communication with respect to better channel conditions ensuring line-of-sights (LoS), Rician fading channel is taken into account. In addition, we consider a more practical case by assuming imperfect CSI at the receiver. More particularly, we derive the analytical approximate expressions for the outage probability and system throughput. To obtain deeper insights, the asymptotic analyses for the outage probability in the high signal-to-noise (SNR) regime and diversity order are performed. Based on the obtained result, an optimal location of the UAV is designed to minimize the average distance between the UAV and users. The main contributions of this work can be summarized as follows:

- We propose a unified framework of HS-UAV NOMA network by using a stochastic geometry approach to model the randomly deployment of ground users. The locations of the ground users follow a homogeneous Poisson point process (PPP) distribution. The probability density functions (PDFs) and the cumulative distribution functions (CDFs) of the user distribution and channel gain between the UAV and the ground users are derived.
- Based on the proposed framework, we derive the approximate analytical closed-form expressions for the outage probability and the system throughput under the delay-limited transmission mode of the random NOMA users in the presence of imperfect CSI. It is shown that there are error floors for the outage probability of the far user and the near user due to channel estimation error.
- We obtain the asymptotic approximate expressions for outage probability of the near user and the far user in the high SNR regime. Furthermore, we obtain and discuss the diversity orders in terms of asymptotic outage probability. It reveals that the derived approximate results remain relatively tight in the moderate and high SNR region.
- To maximize the system performance, we design an optimal location scheme of the UAV by minimizing the average path-loss between the UAV and the ground users. This means that, by carefully designing the location of

This article has been accepted for publication in a future issue of this journal, but has not been fully edited. Content may change prior to final publication. Citation information: DOI 10.1109/ACCESS.2020.2964730, IEEE Access



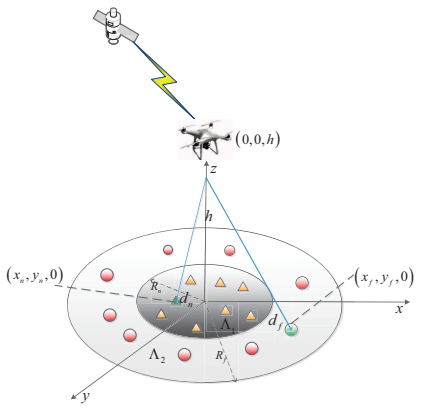


FIGURE 1: system model

the UAV, the outage probability and throughput can be maximized.

### C. ORGANIZATION AND NOTATIONS

The rest of this paper is organized as follows. In Section II, system and channel models of the proposed HS-UAV NOMA networks are presented. Section III first derives the analytical approximate expressions for the outage probability and system throughput of the far user and the near user, then discusses the diversity orders in terms of asymptotic outage probability at high SNRs. Section IV presents the optimization scheme of the location of the UAV. Section V provides the numerical simulation results and key findings before we conclude the paper in Section VI.

Notations: In this paper, $|\cdot|$ denotes the absolute value of a scalar, while $\Pr(X)$ represents the probability of a random variable $X$. In addition, $F(X)$ and $f(X)$ denote the cumulative distribution function (CDF) and the probability density function (PDF), respectively. $\gamma(\cdot\,,\cdot)$ is an incomplete Gamma function and $X!$ denotes the factorial of $X$. Finally, $E[\cdot]$ means the expectation operator of random variables.

## II. SYSTEM MODEL AND FADING MODEL

### A. SYSTEM MODEL

We consider a downlink HS-UAV NOMA network, where one satellite $S$ aims to communicate with terrestrial NOMA users with the aid of a DF UAV relay $U$, as shown in Fig. 1. The UAV is deployed at a constant height $h$. It is assumed that the UAV and all users operate in the half-duplex mode, and all nodes are equipped with single antennas. According to the distances between the UAV and the NOMA users, all the served users are classified into two groups $\Lambda_1$ and $\Lambda_2$. We assume that the near user $D_n$ in group $\Lambda_1$ are located in the circle with radius $R_n$, and the far user $D_f$ in group $\Lambda_2$ are located in ring with inner radius $R_n$ and outer radius $R_f$ ($R_f > R_n$). We also assume that the direct links between the satellite and the users are absent due to the obstacle or severe large-scale fading. In order to obtain higher performance gain, random user pairing is considered. In the following, we will focus on the performance of the paired user, and other pair performance can be obtained using the same methodology.[2]

The entire communication is divided into two time slots: 1) Satellite-to-UAV; 2) UAV-to-Users.

1) The first stage: During the first time slot, $S$ sends superposed signal $y_S = \sqrt{a_1 P_S}x_1 + \sqrt{a_2 P_S}x_2$ to $U$, where $P_S$ is the total power transmitted by $S$; $x_1$ and $x_2$ are corresponding signals of $D_f$ and $D_n$, with $E\left[|x_1|^2\right] = E\left[|x_2|^2\right] = 1$; where $a_1$ and $a_2$ denote the power allocation coefficients for $D_f$ and $D_n$ satisfying $a_1 + a_2 = 1$ and $a_1 > a_2$. Thus, the received signal at the relay can be expressed as

$$y_{SR} = h_{SR}\left(\sqrt{a_1 P_S}x_1 + \sqrt{a_2 P_S}x_2\right) + n_0, \tag{1}$$

where $n_0 \sim CN(0, N_0)$ denotes the additive white Gaussian noise (AWGN).

In practice, it is a great challenge to obtain full knowledge of CSI. The common way is that the receiver estimate the CSI by a training sequence. With this method, the real channel coefficients are affected by the channel estimation error, which can be modeled as $h_i = \hat{h}_i + e_i$, $i = \{SR, RD_n, RD_f\}$, where $h_i$ and $\hat{h}_i$ represent real and estimated channel coefficients, respectively; $e_i \sim CN\left(0, \sigma_{e_i}^2\right)$ denotes the channel estimation error which can be approximated as a complex Gaussian random variable [25]. Therefore, the received signals at the relay can be re-expressed as

$$y_{SR} = \left(\hat{h}_{SR} + e_{SR}\right)\left(\sqrt{a_1 P_S}x_1 + \sqrt{a_2 P_S}x_2\right) + n_0. \tag{2}$$

According to NOMA protocol, SIC is applied at $U$ to decode $D_f$'s signal $x_1$ first, and then $x_2$ will be decoded. Therefore, the received signal-to-interference-plus-noise ratios (SINRs) of the signals $x_1$ and $x_2$ at $U$ are expressed as

$$\gamma_{x_1}^{SR} = \frac{\rho_{SR} a_1 \gamma}{\rho_{SR} a_2 \gamma + \sigma_{e_{SR}}^2 \gamma + 1}, \tag{3}$$

$$\gamma_{x_2}^{SR} = \frac{\rho_{SR} a_2 \gamma}{\sigma_{e_{SR}}^2 \gamma + 1}, \tag{4}$$

where $\gamma = \frac{P_S}{N_0}$ is the transmit SNR at $S$ and $\rho_{SR} = |\hat{h}_{SR}|^2$ is the channel gain.

2) The second stage: During the second time slot, $U$ decodes and forwards the received signal to the paired users at the same time, and the received signal at $D_f$ and $D_n$ are expressed as

$$y_{RD_f} = \left(\hat{h}_{RD_f} + e_{RD_f}\right)\left(\sqrt{b_1 P_R}x_1 + \sqrt{b_2 P_R}x_2\right) + n_f, \tag{5}$$

$$y_{RD_n} = \left(\hat{h}_{RD_n} + e_{RD_n}\right)\left(\sqrt{b_1 P_R}x_1 + \sqrt{b_2 P_R}x_2\right) + n_n, \tag{6}$$

where $P_R$ is the total transmitted power of $U$; $b_1$ and $b_2$ are the power allocation coefficients of the relay transmitted to $D_f$ and $D_n$ with $b_1 + b_2 = 1$ and $b_1 > b_2$; $n_f \sim CN(0, N_f)$

[2]It is noted that some user pairing algorithms are capable of further improving the system performance, which is set aside our ongoing work.

This article has been accepted for publication in a future issue of this journal, but has not been fully edited. Content may change prior to final publication. Citation information: DOI 10.1109/ACCESS.2020.2964730, IEEE Access



and $n_n \sim CN(0, N_n)$ denote the additive white Gaussian noise (AWGN). The signals $x_1$ and $x_2$ are decoded and forwarded to $D_f$ and $D_n$ by $U$, respectively. Thus, the received SINR at $D_f$ is expressed as

$$\gamma_{x_1}^{RD_f} = \frac{\rho_{RD_f} b_1 \gamma_1}{\rho_{RD_f} b_2 \gamma_1 + \sigma_{e_{RD_f}}^2 \gamma_1 + 1}, \tag{7}$$

where $\gamma_1 = \frac{P_R}{N_f}$ is the transmit SNR to $D_f$ at $U$ and $\rho_{RD_f} = |\hat{h}_{RD_f}|^2$ is the channel gain.

According to the SIC, the SINRs for $D_n$ to decode the desired signal and $D_f$'s signal are expressed as

$$\gamma_{x_2}^{RD_n} = \frac{\rho_{RD_n} b_2 \gamma_2}{\sigma_{e_{RD_n}}^2 \gamma_1 + 1}, \tag{8}$$

$$\gamma_{x_1}^{RD_n} = \frac{\rho_{RD_n} b_1 \gamma_2}{\rho_{RD_n} b_2 \gamma_1 + \sigma_{e_{RD_n}}^2 \gamma_2 + 1}, \tag{9}$$

where $\rho_{RD_n} = |\hat{h}_{RD_n}|^2$ is the channel gain; $\gamma_2 = \frac{P_R}{N_n}$ is the transmit SNR to $D_n$ at $U$.

### B. FADING MODEL

To ensure the better channel conditions, the LoS links exist between the UAV and the users. In light of this fact, Rician fading is taken into account [26]. In addition, the link between satellite and UAV is assumed to follow Rician distribution.[3]

The channel coefficient $h_j$, $j = \{RD_n, RD_f\}$, from UAV to the paired NOMA users $D_m$, $m = \{n, f\}$, are denoted as

$$h_j = \frac{\hat{h}_j}{\sqrt{1 + d_m^{\nu}}}, \tag{10}$$

where $\nu$ is the path loss exponent and $d_m$ denotes the distance between the UAV and the paired NOMA user $D_m$; the coordinates of $m$-th users $D_m$ and UAV are represented by $(x_m, y_m, 0)$ and $(0, 0, h)$. Thus, the distance $d_m$ can be denoted as

$$d_m = \sqrt{x_m^2 + y_m^2 + h^2}. \tag{11}$$

It is obvious that the distance counts on the location of the UAV and the paired NOMA users. We assume that all users located in $\Lambda_1$ and $\Lambda_2$ follow a homogeneous PPP. Therefore, the NOMA users are modeled as independently and identically distributed points in $\Lambda_1$ and $\Lambda_2$, denoted by $\omega_m$, and PDFs of $\omega_n$ and $\omega_f$ are given by

$$f_{\omega_n}(\omega_n) = \frac{1}{\pi R_n^2}, \tag{12}$$

and

$$f_{\omega_f}(\omega_f) = \frac{1}{\pi\left(R_f^2 - R_n^2\right)}, \tag{13}$$

respectively.

[3]In fact, Rician shadow has been the prevalent model to capture the characterization of satellite communication systems, our results however can be extended to other fading model.

As discussed above, the link between the satellite and the UAV follows a Rician distribution, and the PDF of the channel gain $\rho_i$ can be expressed as

$$f_{\rho_i}(x) = \frac{(K+1)e^{-K}}{\lambda_i} e^{-\frac{K+1}{\lambda_i}x} I_0\left(2\sqrt{\frac{K(K+1)x}{\lambda_i}}\right), \tag{14}$$

where $\lambda_i$ is the mean value of $\rho_i$; $K$ is the Rician factor, which is defined as the ratio of the power of the LoS component to the scattered components and $I_0(\cdot)$ denotes the zeroth order modified Bessel function of the first kind [27]. The corresponding CDF is given by

$$F_{\rho_i}(x) = 1 - \mathcal{Q}\left(\sqrt{2K}, \sqrt{\frac{2(K+1)x}{\lambda_i}}\right), \tag{15}$$

where $\mathcal{Q}(a, b) \triangleq \int_b^{\infty} x e^{-\frac{a^2+x^2}{2}} I_0(ax) dx$ is the Marcum Q-function of first order [28].

Unfortunately, it is difficult, if not impossible, to obtain the exact performance of the considered network. To solve this issue, we use the equality $I_0(x) = \sum_{l=1}^{\infty} \frac{x^l}{2^{2l}(l!)^2}$ [29], hence the PDF of the channel gain $\rho_i$ can be re-expressed as

$$f_{\rho_i}(x) = \frac{(K+1)e^{-K}}{\lambda_i} \sum_{l=0}^{\infty} \frac{x^l}{(l!)^2} \left(\frac{K(K+1)}{\lambda_i}\right)^l e^{-\frac{K+1}{\lambda_i}x}. \tag{16}$$

Based on the above formulas, we can get the CDF of the channel gain $\rho_i$ as

$$F_{\rho_i}(x) = 1 - e^{-K} \sum_{l=0}^{\infty} \sum_{m=0}^{l} \frac{K^l}{l!m!} \left(\frac{K+1}{\lambda_i}\right)^m x^m e^{-\frac{K+1}{\lambda_i}x}. \tag{17}$$

To evaluate the performance of the user modelled by a PPP, we first obtain the closed-form expressions of the CDF for $|h_n|^2$ and $|h_f|^2$, which are provided in the following proposition.

**Proposition 1.** *Suppose all users follow a homogeneous PPP, using stochastic geometry, the CDF of the squared channel gain $|h_n|^2$ and $|h_f|^2$ are given by*

$$F_{|h_n|^2}(x) = 1 - \frac{2}{R_n^2} e^{-\frac{(K+1)x}{\lambda_i} - K} \sum_{l=0}^{\infty} \sum_{m=0}^{l} \frac{K^l}{l!m!} \left(\frac{K+1}{\lambda_i}\right)^m x^m \times \sum_{t=0}^{m} \binom{m}{t} \nu^{-1} \left(\frac{(K+1)x}{\lambda_i}\right)^{-\frac{\nu t+2}{\nu}} \gamma\left(\frac{\nu t+2}{\nu}, \frac{(K+1)x}{\lambda_i} R_n^{\nu}\right), \tag{18}$$

*and (19), shown at the top of the next page.*

*Proof.* Based on (12) and (17), for an arbitrary choice of $\nu$, the CDF of $|h_n|^2$ is given by (20), shown at the top of the next page.

After some manipulations, (18) can be obtained.

Similarly, for an arbitrary choice of $\nu$, the CDF of $|h_f|^2$ can be expressed as in (21), shown at the top of the next page.

After some manipulations, (19) can be proved. □

This article has been accepted for publication in a future issue of this journal, but has not been fully edited. Content may change prior to final publication. Citation information: DOI 10.1109/ACCESS.2020.2964730, IEEE Access



$$F_{|h_f|^2}(x)=1-\sum_{l=0}^{\infty}\sum_{m=0}^{l}\sum_{t=0}^{m}\binom{m}{t}\frac{K^l}{l!m!}\times\left(\frac{K+1}{\lambda_i}\right)^m\frac{2x^m}{R_f^2-R_n^2}e^{-\frac{K+1}{\lambda_i}x-K}\times\nu^{-1}\left(\frac{(K+1)x}{\lambda_i}\right)^{-\frac{\nu t+2}{\nu}}\left(\gamma\left(\frac{\nu t+2}{\nu},\frac{(K+1)x}{\lambda_i}R_f^{\nu}\right)-\gamma\left(\frac{\nu t+2}{\nu},\frac{(K+1)x}{\lambda_i}R_n^{\nu}\right)\right) \tag{19}$$

$$\begin{aligned}F_{|h_n|^2}(x)&=\int_{I_n}\left(1-e^{-K}\sum_{l=0}^{\infty}\sum_{m=0}^{l}\frac{K^l}{l!m!}\left(\frac{K+1}{\lambda_i}\right)^m x^m(1+d^{\nu})^m e^{-\frac{K+1}{\lambda_i}x(1+d^{\nu})}\right)f_{\omega_n}(\omega_n)\,d\omega_n\\&=\frac{2}{R_n^2}\int_0^{R_n}rdr-\frac{2}{R_n^2}\int_0^{R_n}e^{-K}\sum_{l=0}^{\infty}\sum_{m=0}^{l}\frac{K^l}{l!m!}\left(\frac{K+1}{\lambda_i}\right)^m x^m(1+r^{\nu})^m e^{-\frac{K+1}{\lambda_i}x(1+r^{\nu})}rdr\end{aligned} \tag{20}$$

$$\begin{aligned}F_{|h_f|^2}(x)&=\int_{I_f}\left(1-e^{-K}\sum_{l=0}^{\infty}\sum_{m=0}^{l}\frac{K^l}{l!m!}\left(\frac{K+1}{\lambda_i}\right)^m x^m(1+d^{\nu})^m e^{-\frac{K+1}{\lambda_i}x(1+d^{\nu})}\right)f_{\omega_f}(\omega_f)\,d\omega_f\\&=\frac{2}{R_f^2-R_n^2}\int_{R_n}^{R_f}\left(1-e^{-K}\sum_{l=0}^{\infty}\sum_{m=0}^{l}\frac{K^l}{l!m!}\left(\frac{K+1}{\lambda_i}\right)^m x^m(1+r^{\nu})^m e^{-\frac{K+1}{\lambda_i}x(1+r^{\nu})}r\right)dr\end{aligned} \tag{21}$$

## III. OUTAGE PROBABILITY ANALYSIS

In this section, we carry out the outage performance analysis for the paired NOMA users, $D_f$ and $D_n$. In order to obtain deeper insights, the asymptotic analysis and diversity order are calculated and analyzed.

### A. OUTAGE PROBABILITY

For the far user $D_f$, the outage event will occur in the following three cases: 1) The relay cannot successfully decode $x_1$; 2) The relay cannot successfully decode $x_2$; 3) The relay can successfully decode $x_1$ and $x_2$ while $D_f$ cannot successfully decode its signal. Therefore, the OP of the far user $D_f$ can be expressed as

$$P_{out}^{D_f}=\Pr\left(\min\left(\frac{\gamma_{x_1}^{SR}}{\gamma_{th,f}},\frac{\gamma_{x_2}^{SR}}{\gamma_{th,n}},\frac{\gamma_{x_1}^{RD_f}}{\gamma_{th,f}}\right)<1\right), \tag{22}$$

where $\gamma_{th,f}$ and $\gamma_{th,n}$ are the outage thresholds at $D_f$ and $D_n$, respectively. In the following theorem, the approximate expression for OP of $D_f$ will be presented.

**Theorem 1.** *The approximate closed-form expression for the OP of $D_f$ can be expressed as (23), shown at the top of the next page.*

*where* $\zeta_1=\frac{\sigma_{e_{SR}}^2\gamma\gamma_{th,f}+\gamma_{th,f}}{a_1\gamma-a_2\gamma\gamma_{th,f}}$, $\zeta_2=\frac{\sigma_{e_{SR}}^2\gamma\gamma_{th,n}+\gamma_{th,n}}{a_2\gamma}$, $\zeta=\max(\zeta_1,\zeta_2)$ *and* $\psi=\frac{\sigma_{e_{RD_f}}^2\gamma_1\gamma_{th,f}+\gamma_{th,f}}{b_1\gamma_1-b_2\gamma_1\gamma_{th,f}}$.

*Proof.* See Appendix A. □

For the near user $D_n$, the outage events will not occur until both the relay and the near user $D_n$ decode $x_1$ and $x_2$ successfully. Thus, the approximate OP of $D_n$ will be expressed as

$$\begin{aligned}P_{out}^{D_n}&=\Pr\left(\min\left(\frac{\gamma_{x_1}^{SR}}{\gamma_{th,f}},\frac{\gamma_{x_2}^{SR}}{\gamma_{th,n}}\right)<1\right)\\&+\Pr\left(\min\left(\frac{\gamma_{x_1}^{SR}}{\gamma_{th,f}},\frac{\gamma_{x_2}^{SR}}{\gamma_{th,n}}\right)\geq 1,\min\left(\frac{\gamma_{x_1}^{RD_n}}{\gamma_{th,f}},\frac{\gamma_{x_2}^{RD_n}}{\gamma_{th,n}}\right)<1\right).\end{aligned} \tag{24}$$

The approximate closed-form expression of the OP for the near user will be provided in the following theorem.

**Theorem 2.** *The approximate closed-form expression for the OP of $D_n$ can be expressed as (25), shown at the top of the next page.*

*where* $\phi_1=\frac{\sigma_{e_{RD_n}}^2\gamma_1\gamma_{th,f}+\gamma_{th,f}}{b_1\gamma_1-b_2\gamma_1\gamma_{th,f}}$, $\phi_2=\frac{\sigma_{e_{RD_n}}^2\gamma_1\gamma_{th,n}+\gamma_{th,n}}{b_2\gamma_1}$ *and* $\phi=\max(\phi_1,\phi_2)$.

*Proof.* See Appendix B. □

### B. ASYMPTOTIC OUTAGE PROBABILITY

To gain more insights, we focus on the asymptotic analysis for the OP in the high SNR region. As in [30], at the high SNRs, Marcum Q- function can be approximated as

$$\mathcal{Q}\left(\sqrt{2K},\sqrt{\frac{2(K+1)x}{\lambda_i}}\right)\approx 1-e^{-K}\frac{(K+1)x}{\lambda_i}, \tag{26}$$

and the CDF of (17) can be further approximated by

$$F_{\rho_i}^{\infty}(x)\approx e^{-K}\frac{(1+K)x}{\lambda_i}. \tag{27}$$

Next, the asymptotic analysis will be provided in the following corollaries.

This article has been accepted for publication in a future issue of this journal, but has not been fully edited. Content may change prior to final publication. Citation information: DOI 10.1109/ACCESS.2020.2964730, IEEE Access



$$P_{out}^{D_f}=1-\sum_{l_1=0}^{\infty}\sum_{m_1=0}^{l_1}\sum_{l_2=0}^{\infty}\sum_{m_2=0}^{l_2}\sum_{t=0}^{m_2}\binom{m_2}{t}\frac{K^{l_1+l_2}}{l_1!l_2!m_1!m_2!}\left(\frac{K+1}{\lambda_{SR}}\right)^{m_1}\left(\frac{K+1}{\lambda_{RD_f}}\right)^{m_2}\frac{2\zeta^{m_1}\psi^{m_2}}{R_f^2-R_n^2}$$
$$\times e^{-\frac{K+1}{\lambda_{SR}}\zeta-\frac{K+1}{\lambda_{RD_f}}\psi-2K}\left(\gamma\left(\frac{\nu t+2}{\nu},\frac{(K+1)\psi}{\lambda_i}R_f^{\nu}\right)-\gamma\left(\frac{\nu t+2}{\nu},\frac{(K+1)\psi}{\lambda_i}R_n^{\nu}\right)\right)\nu^{-1}\left(\frac{(K+1)\psi}{\lambda_{RD_f}}\right)^{-\frac{\nu t+2}{\nu}} \tag{23}$$

$$P_{out}^{D_n}=1-\sum_{l_1=0}^{\infty}\sum_{m_1=0}^{l_1}\sum_{l_3=0}^{\infty}\sum_{m_3=0}^{l_3}\sum_{t=0}^{m_3}\binom{m_3}{t}\frac{K^{l_1+l_3}}{l_1!l_3!m_1!m_3!}\left(\frac{K+1}{\lambda_{SR}}\right)^{m_1}\left(\frac{K+1}{\lambda_{RD_n}}\right)^{m_3}$$
$$\times\frac{2\zeta^{m_1}\phi^{m_3}}{R_n^2}e^{-\frac{K+1}{\lambda_{SR}}\zeta-\frac{(K+1)\phi}{\lambda_{RD_n}}-2K}\nu^{-1}\left(\frac{(K+1)\phi}{\lambda_{RD_n}}\right)^{-\frac{\nu t+2}{\nu}}\gamma\left(\frac{\nu t+2}{\nu},\frac{(K+1)\phi}{\lambda_{RD_n}}R_n^{\nu}\right) \tag{25}$$

**Corollary 1.** *At high SNRs, the asymptotic closed-form of OP for $D_f$ is given as*

$$P_{D_f}^{\infty}=1-\left(1-e^{-K}\frac{(1+K)\zeta}{\lambda_1}\right)\times\left(1-\frac{(1+K)\psi e^{-K}}{\lambda_3}\left(1+\frac{2\left(R_f^{\nu+2}-R_n^{\nu+2}\right)}{(\nu+2)\left(R_f^2-R_n^2\right)}\right)\right). \tag{28}$$

*Proof.* See Appendix C. □

**Corollary 2.** *At high SNRs, the asymptotic closed-form of the OP for $D_n$ is given as*

$$P_{D_n}^{\infty}=1-\left(1-e^{-K}\frac{(1+K)\zeta}{\lambda_1}\right)\times\left(1-\frac{(1+K)\phi e^{-K}}{\lambda_2}\left(1+\frac{2R_n^{\nu}}{\nu+2}\right)\right). \tag{29}$$

*Proof.* See Appendix D. □

### C. DIVERSITY ORDER

Based on the derived asymptotic results, we will focus on the diversity order in the high SNR regime, which is defined as in [31]

$$d=-\lim_{\gamma'\to\infty}\frac{\log\left(P_{out}^{\infty}\right)}{\log\gamma'}, \tag{30}$$

where $\gamma'\in\{\gamma_1,\gamma_2\}$ is transmitted SNR and $P_{out}^{\infty}$ is the asymptotic OP.

**Corollary 3.** *The diversity order of $D_f$ is given as*

$$d_f=-\lim_{\gamma_1\to\infty}\frac{\log\left(P_{D_f}^{\infty}\right)}{\log\gamma_1}=0. \tag{31}$$

**Corollary 4.** *The diversity order of $D_n$ is given as*

$$d_n=-\lim_{\gamma_2\to\infty}\frac{\log\left(P_{D_n}^{\infty}\right)}{\log\gamma_2}=0. \tag{32}$$

**Remark 1.** *From Corollary 3 and Corollary 4, we can observe that the diversity orders of the far and near users in the high SNR regime are zero. This happens because the asymptotic OP is fixed as a non-zero constant due to channel estimation error. This means that the average power is not always beneficial to the system outage performance under the condition of imperfect CSI.*

### D. SYSTEM THROUGHPUT

In wireless communication networks, system throughput is another significant metric to evaluate the system performance. It is defined as the product of the reliable communication and the data rate. Moreover, there are two transmission modes of operation in wireless communication systems: (1) delay-tolerant transmission mode; (2) delay-limited transmission mode. In the delay-tolerant transmission mode, the systems operate under the condition of error free, and the system throughput is determined by the ergodic rate. In the delay-limited transmission mode, the systems operate under a fixed rate, and the system throughput is determined by the wireless fading channels. In this paper, the delay-limited transmission mode is considered, and the system throughput is given as[4]

$$R=\sum\nolimits_{i=1}^{M}\left(1-p_{D_m}\right)\times R_{th,m}, \tag{33}$$

where $R_{th,m}$ denotes the transmission date rate of $D_m$ and can be expressed as $R_{th,m}=\frac{1}{2}\log_2\left(1+\gamma_{th,m}\right)$, the constant $1/2$ represents that the communication process is divided into two time slots and $\gamma_{th,m}$ indicates the outage threshold of user $D_m$.

## IV. LOCATION OPTIMIZATION

As shown in (10), for the fixed transmission power, the OPs for the paired users $D_n$ and $D_f$ highly rely on the distance between the UAV and the user.[5] Considering this fact, we design an optimal deployment scheme to maximize the sum rate of the proposed system under the condition of desired quality-of-service (QoS). This can be achieved by minimizing the average path-loss by shortening the average distances between the UAV and all NOMA users.[6] In this

[4]Although we focus on the system throughput of delay-limited transmission mode, our results can be easily extended to the delay-tolerant transmission mode.

[5]In fact, the path-loss is a determined factor since that multiple path fading and shadowing fading revolves around the path-loss [32].

[6]Note that the change of position of the UAV for the satellite is negligible due to long distance between the satellite and the UAV. Therefore, for the location optimization, we only focus on the link between the UAV and users.

This article has been accepted for publication in a future issue of this journal, but has not been fully edited. Content may change prior to final publication. Citation information: DOI 10.1109/ACCESS.2020.2964730, IEEE Access



TABLE 1: Table of parameters for numerical results

| | |
|---|---|
| Monte Carlo simulations | $10^7$ iterations |
| The power allocation coefficients of $P_S$ | $a_1 = 0.7, a_2 = 0.3$ |
| The power allocation coefficients of $P_R$ | $b_1 = 0.8, b_2 = 0.2$ |
| The mean square error of channel estimation error | $\sigma_{e_{SR}} = \sigma_{e_{RD_f}} = \sigma_{e_{RD_n}} = 0.07$ |
| The variance of the additive white Gaussian noise (AWGN) | $N_0 = N_f = N_n = 1$ |
| The Rician channel parameter | $K = 1$ |
| The radius of inner circle and outer circle | $R_n = 0.2m, R_f = 0.8m$ |
| The height of UAV | $h = 100m$ |
| The path loss exponent | $\upsilon = 3$ |
| The outage threshold | $\gamma_{th_f} = 0.01, \gamma_{th_n} = 1$ |

regard, we formulate the constrained optimization problem for location optimization as follows

$$\begin{aligned}(P_1)\ &\max_{X_u, Y_n} \sum_{k=1}^{M} \log_2\left(1+\gamma_k\right),\\ &C_1: \log_2\left(1+\gamma_{th,n}\right) > \zeta_n,\\ &C_2: \log_2\left(1+\gamma_{th,f}\right) > \zeta_f,\\ &C_3: \sum\nolimits_{k=1}^{M} a_k = 1,\\ &C_4: \min\left\{x_k\right\} \le X_U \le \max\left\{x_k\right\}, 1 \le k \le M,\\ &C_5: \min\left\{y_k\right\} \le Y_U \le \max\left\{y_k\right\}, 1 \le k \le M, \end{aligned} \tag{34}$$

where $\zeta_n = \log_2\left(1+\gamma_{th,n}\right)$ and $\zeta_f = \log_2\left(1+\gamma_{th,f}\right)$ are the minimum rate of the paired users $D_n$ and $D_f$, respectively; $(x_k, y_k)$ is the coordinate of $k$-th user; and $M$ is the total number of users. To ensure the coverage of UAV, we assume that the UAV stays at a fixed height, and the coordinate of the UAV is $(X_U, Y_U, h)$. To solve the problem $(P_1)$, we first have the following proposition.

**Proposition 2.** *Under the conditions of a fixed transmit average power, the problem $(P_1)$ is an increasing function with respect to $\rho_{RD_i}$ for $\rho_{RD_i} \ge 0$.*

*Proof.* The proof can be divided into two cases:

*1)* When (7) or (9) is considered, the rate can be represented as a unified form as

$$f\left(x\right) = \log_2\left(1 + \frac{\Theta_1 x}{\Theta_2 x + \Theta_3}\right), \tag{35}$$

where $x \in \left\{\rho_{RD_f}, \rho_{RD_n}\right\}$, $\Theta_1 = b_1\gamma_1$, $\Theta_2 = b_2\gamma_2$ and $\Theta_3 \in \left\{\sigma^2_{e_{RD_f}}\gamma_1 + 1,\ \sigma^2_{e_{RD_n}}\gamma_1 + 1\right\}$.

*2)* When (8) is considered, the rate can be represented as a unified form as

$$f\left(x\right) = \log_2\left(1 + \Delta x\right), \tag{36}$$

where $\Delta = b_2\gamma_1 \Big/ \left(\sigma^2_{e_{RD_n}}\gamma_1 + 1\right)$.

For the first case, we can find that the function $f\left(x\right)$ is an increasing function with respect to $x$ since the first-order derivative function of $f\left(x\right)$ is positive, which is presented as follows

$$f'\left(x\right) = \frac{\Theta_1\Theta_3}{\left(\left(\Theta_1+\Theta_2\right)x + \Theta_3\right)\left(\Theta_2 x + \Theta_3\right)} > 0. \tag{37}$$

For the second case, we have the same result by similar methodology.

Therefore, we have the conclusion of Proposition 2. □

Based on (10), the problem is equivalent to the following one:

$$\begin{aligned}(P_2)\ &\min_{X_U, Y_U} \sum_{k=1}^{M} d_k, \\ &s.t.\ C1: \min\left\{x_k\right\} \le X_U \le \max\left\{x_k\right\}, 1 \le k \le M,\\ &\quad C_2: \min\left\{y_k\right\} \le Y_U \le \max\left\{y_k\right\}, 1 \le k \le M,\end{aligned} \tag{38}$$

where $d_k$ is the distance between the $k$-th user and the UAV. The distance $d_k$ can be expressed as

$$d_k = \sqrt{h^2 + \left(X_U - x_k\right)^2 + \left(Y_U - y_k\right)^2}. \tag{39}$$

To obtain the optimal location of the proposed framework, the derived result is provided in the following theorem.

**Theorem 3.** *The optimal coordinates $X_U^*$ and $Y_U^*$ of the UAV are given as*

$$\begin{aligned} X_U^* &= \sum_{k=1}^{M} \frac{x_k}{M},\\ Y_U^* &= \sum_{k=1}^{M} \frac{y_k}{M}. \end{aligned} \tag{40}$$

*Proof.* See Appendix E. □

**Remark 2.** *From Theorem 3, we can conclude that the sum rate can be maximized by carefully designing optimal location of the UAV, and the optimal x-coordinate and y-coordinate of the UAV are the mean of the x-coordinate and y-coordinate of all the users, respectively.*

## V. NUMERICAL RESULTS

In this section, we evaluate the OP, throughput and optimal UAV location performances via numerical results. The complementary performance evaluation results obtained by means of Monte-Carlo computer simulation trials is presented to verify the accuracy of the theoretical analysis in Sections III and IV. Unless otherwise stated, we use the parameter settings shown in Table 1.

Fig. 2 depicts results of the OP versus the average SNR of the far and near users. For the sake of comparison, the curves for the OP under ideal conditions ($\sigma_{e_{SR}} = \sigma_{e_{RD_n}} = \sigma_{e_{RD_f}} = 0$) is provided. From Fig. 2, one can observe

This article has been accepted for publication in a future issue of this journal, but has not been fully edited. Content may change prior to final publication. Citation information: DOI 10.1109/ACCESS.2020.2964730, IEEE Access



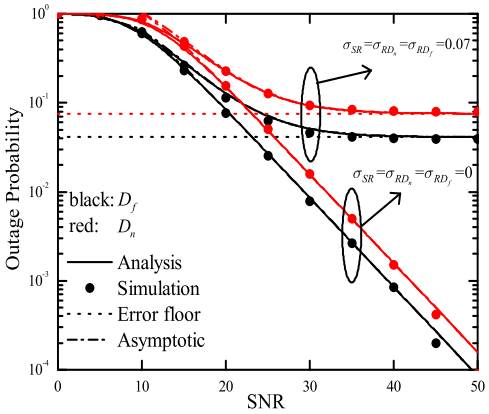


FIGURE 2: OP of the far and near users for different channel estimation errors vs. transmit SNR

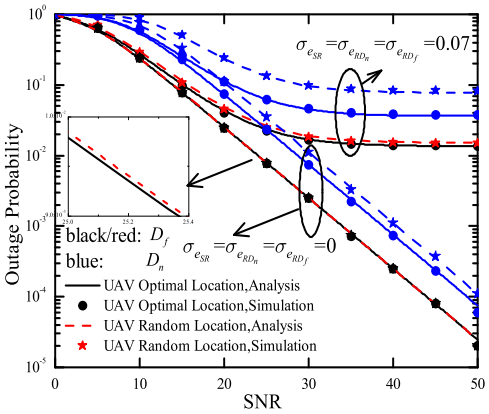


FIGURE 3: OP of UAV for different channel estimation errors in optimal location vs. random location

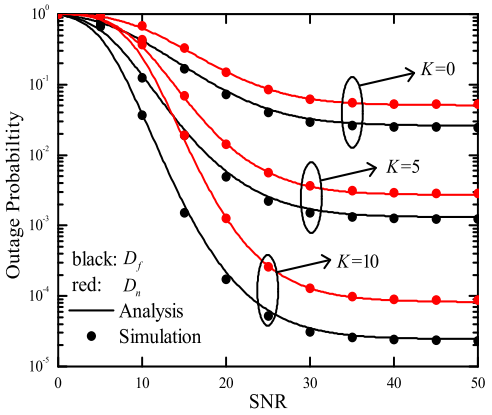


FIGURE 4: OP in different Rician factors

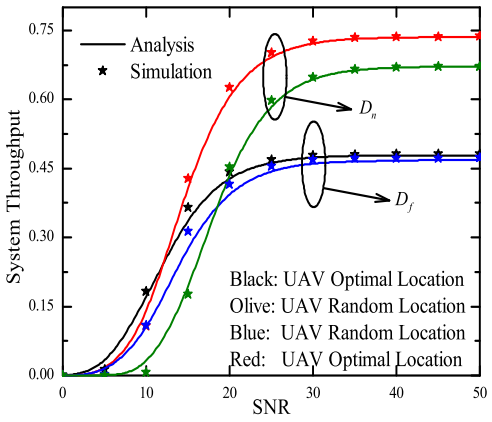


FIGURE 5: System Throughput of UAV in optimal location vs. random location

that the theoretical analytical results of (23), (25) and (28), (29) match with the simulated results, which verified the correctness of our analysis. Moreover, one can also observe that the curves of the analytical OP almost overlap with the asymptotic result in terms of outage probability in the moderate and high SNR region. This figure also indicates that there are error floors for the OP at high SNRs because of the channel estimate error, which verifies the conclusion in Remark 1. This means that we cannot improve the outage probability by increasing the average SNR. However, under ideal conditions, the average SNR is always beneficial to the OP.

Fig. 3 plots the OP of the far and the near users versus the average SNR for different channel estimation errors $\sigma_{e_i}$. In this simulation, we consider two scenarios for the UAV: 1) optimal location; 2) random location. As one can see, the curves of theoretical analysis sufficiently coincide with the Monte Carlo curves for the two scenarios. Furthermore, the outage performance of the first scenario outperforms that of the second scenario, which implies that the proposed location optimization scheme can minimize the OP. Finally, we can also observe that the near user is more sensitive to the location of UAV than that of the far user.

In Fig. 4, we show the OP versus the average SNR for different Rician factors $K = \{0,\ 5,\ 10\}$. When Rician factor is 0 ($K$=0), the Rician fading reduces to the Rayleigh fading. It can be seen that for an increase in the values of $K$, the OP declines, whereas for small values of $K(K$=0) the OP increases. This means that for large $K(K$=10), there is a strong LoS condition to support the communication, which yields good outage performance. It can also be seen that there are error floors for the outage probability for all Rician factor settings due to channel estimation error. It indicates that UAV communication can provide reliability communication. Finally, we note that the derived approximate expressions remain sufficient tight for the whole SNR range.

In Fig. 5, we have compared the proposed optimization scheme with the random UAV deployment scheme. From Fig. 5, we note that the system throughput with optimal location scheme outperforms the random UAV scheme since the optimization scheme has the smallest path-loss caused by the shortest average distance between the UAV and users. Similar results can be seen that there exist ceilings for the

This article has been accepted for publication in a future issue of this journal, but has not been fully edited. Content may change prior to final publication. Citation information: DOI 10.1109/ACCESS.2020.2964730, IEEE Access



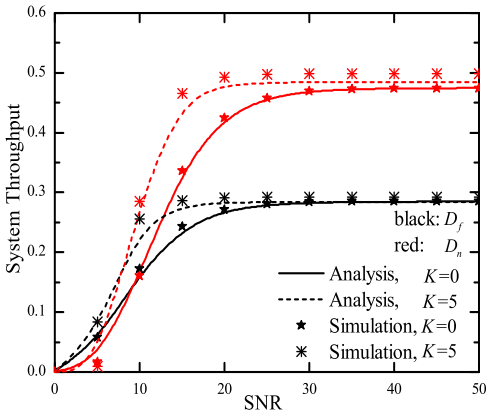


FIGURE 6: Throughput in different Rician factors

system throughput at high SNRs due to the fixed constant for the OP caused by channel estimation error. We have observed that the OP of the near user is superior to the far user from Fig. 2. According to the relationship between throughput and OP, which is that the larger the OP, the smaller the throughput, the system throughput of the near user should be superior to the far user. The curves of system throughput for the near user is above that for the far user in Fig. 5. This result verifies the validity of the theoretical analysis.

Fig. 6 shows system throughput versus transmit SNR for different Rician factors $K=\{0,\ 5\}$. As stated before, when Rician factor is 0, the fading channel reduces to the Rayleigh fading channel. We note that the throughput tends to a fixed constant as the average SNR grows large. This happens because at high SNRs, there exists an error floor caused by channel estimation error. These results are consistent with Fig. 5. Also, it can be seen that Rician factor has more severe effects on the near user than the far user because of strong LoS. As in Fig. 4, a large value of Rician factor yields a high throughput.

## VI. CONCLUSION

In this paper, the performance of HS-UAV NOMA network over Rician fading channels is studied. Specifically, we derived the analytical approximate expressions for the outage probability and system throughput for the far and near users in the presence of channel estimation error. Based on the derived approximations, we explore the asymptotic behavior in the high SNR regime, as well as the diversity orders. We demonstrate that there are floors for the outage probability caused by non-ideal channel estimation. To further improve system performance, we design an optimal location scheme for the UAV. As illustrated by simulation results, the proposed scheme outperforms the random UAV scheme, specifically for the far users.

.

## APPENDIX A: PROOF OF THEOREM 1

The proof starts by simplifying (22) to the following form as

$$\begin{aligned} P_{out}^{D_f} &= 1-\Pr\left(\gamma_{x_1}^{SR}\geq\gamma_{th,f},\gamma_{x_2}^{SR}\geq\gamma_{th,n},\gamma_{x_1}^{RD_f}\geq\gamma_{th,f}\right) \\ &= 1-\Pr\left(\rho_{SR}\geq\zeta\right)\Pr\left(\rho_{RD_f}\geq\psi\right) \\ &= 1-\left(1-F_{\rho_{SR}}\left(\zeta\right)\right)\left(1-F_{\rho_{RD_f}}\left(\psi\right)\right). \end{aligned} \tag{A.1}$$

Substituting (17) and (19) into (A.1), we can get (A.2), shown at the top of the next page.

After some algebra operations, we can conclude the proof the Theorem 1.

## APPENDIX B: PROOF OF THEOREM 2

Based on (24), the near user $D_n$ can be simplified to (B.1), shown at the top of the next page.

Substituting (17) and (18) into (B.1), we can get (B.2), shown at the top of the next page.

After some algebra operations, we can conclude the proof of Theorem 2.

## APPENDIX C: PROOF OF COROLLARY 1

Combined (13) with (27), the CDF of $|h_f|^2$ is approximated by

$$F_{|h_f|^2}\left(x\right)\approx\frac{\left(1+K\right)xe^{-K}}{\lambda_i}\left(1+\frac{2\left(R_f^{\nu+2}-R_n^{\nu+2}\right)}{(\nu+2)\left(R_f^2-R_n^2\right)}\right). \tag{C.1}$$

Substituting (27) and (C.1) into (A.1), we can obtain

$$\begin{aligned} P_{D_f}^{\infty} &= 1-\left(1-e^{-K}\frac{(1+K)\zeta}{\lambda_1}\right) \\ &\times\left(1-\frac{(1+K)\psi e^{-K}}{\lambda_3}\left(1+\frac{2\left(R_f^{\nu+2}-R_n^{\nu+2}\right)}{(\nu+2)\left(R_f^2-R_n^2\right)}\right)\right). \end{aligned} \tag{C.2}$$

## APPENDIX D: PROOF OF COROLLARY 2

Combined (12) with (27), the CDF of the squared channel gain $|h_n|^2$ is approximated by

$$F_{|h_n|^2}\left(x\right)\approx\frac{\left(1+K\right)xe^{-K}}{\lambda_i}\left(1+\frac{2R_n^{\nu}}{\nu+2}\right). \tag{D.1}$$

Substituting (27) and (D.1) into (B.1), we can obtain (D.2).

$$\begin{aligned} P_{D_n}^{\infty} &= 1-\left(1-e^{-K}\frac{(1+K)\zeta}{\lambda_1}\right) \\ &\times\left(1-\frac{(1+K)\phi e^{-K}}{\lambda_2}\left(1+\frac{2R_n^{\nu}}{\nu+2}\right)\right). \end{aligned} \tag{D.2}$$

## APPENDIX E:PROOF OF THEOREM 3

For the problem $(P_2)$, based on (39), the problem $(P_2)$ is equivalent to

$$\begin{aligned} (P_3)\quad &\min_{X_U,Y_U}\sum_{k=1}^{M}\left(X_U-x_k\right)^2+\left(Y_U-y_k\right)^2 \\ &s.t.\ \min\left\{x_i\right\}\leq X_U\leq\max\left\{x_i\right\},1\leq i\leq M \\ &\min\left\{y_j\right\}\leq Y_U\leq\max\left\{y_j\right\},1\leq j\leq M. \end{aligned} \tag{E.1}$$

We note that $(P_3)$ is a convex function with respect to $X_U$ and $Y_U$ since the second derivative of $X_U$ or $Y_U$ is $2M>0$. Moreover, the constraint conditions of $(P_3)$ are

This article has been accepted for publication in a future issue of this journal, but has not been fully edited. Content may change prior to final publication. Citation information: DOI 10.1109/ACCESS.2020.2964730, IEEE Access



$$P_{out}^{D_f} = 1 - e^{-K} \sum_{l_1=0}^{\infty} \sum_{m_1=0}^{l_1} \frac{K^{l_1}}{l_1! m_1!} \left(\frac{K+1}{\lambda_{SR}}\right)^{m_1} \zeta^{m_1} e^{-\frac{K+1}{\lambda_{SR}}\zeta} \frac{2}{R_f^2 - R_n^2} e^{-K} \sum_{l_2=0}^{\infty} \sum_{m_2=0}^{l_2} \frac{K^{l_2}}{l_2! m_2!} \left(\frac{K+1}{\lambda_{RD_f}}\right)^{m_2} \psi^{m_2} e^{-\frac{K+1}{\lambda_{RD_f}}\psi} \times \sum_{t=0}^{m_2} \binom{m_2}{t} \left(\gamma\left(\frac{\nu t+2}{\nu}, \frac{(K+1)\psi}{\lambda_i} R_f^{\nu}\right) - \gamma\left(\frac{\nu t+2}{\nu}, \frac{(K+1)\psi}{\lambda_i} R_n^{\nu}\right)\right) \nu^{-1} \left(\frac{(K+1)\psi}{\lambda_{RD_f}}\right)^{-\frac{\nu t+2}{\nu}} \tag{A.2}$$

$$\begin{aligned} P_{out}^{D_n} &= 1 - \Pr\left(\gamma_{x_1}^{SR} \geq \gamma_{th,f}, \gamma_{x_2}^{SR} \geq \gamma_{th,n}\right) \Pr\left(\gamma_{x_1}^{RD_n} \geq \gamma_{th,f}, \gamma_{x_2}^{RD_n} \geq \gamma_{th,n}\right) \\ &= 1 - \Pr\left(\rho_{SR} \geq \zeta\right) \Pr\left(\rho_{RD_n} \geq \phi\right) \\ &= 1 - \left(1 - F_{\rho_{SR}}(\zeta)\right)\left(1 - F_{\rho_{RD_n}}(\phi)\right) \end{aligned} \tag{B.1}$$

$$P_{out}^{D_n} = 1 - \sum_{l_1=0}^{\infty} \sum_{m_1=0}^{l_1} \sum_{l_3=0}^{\infty} \sum_{m_3=0}^{l_3} \sum_{t=0}^{m_3} \binom{m_3}{t} \frac{K^{l_1+l_3}}{l_1! l_3! m_1! m_3!} \left(\frac{K+1}{\lambda_{SR}}\right)^{m_1} \left(\frac{K+1}{\lambda_{RD_n}}\right)^{m_3} \times \frac{2\zeta^{m_1}\phi^{m_3}}{R_n^2} e^{-\frac{K+1}{\lambda_{SR}}\zeta - \frac{(K+1)\phi}{\lambda_{RD_n}} - 2K} \nu^{-1} \left(\frac{(K+1)\phi}{\lambda_{RD_n}}\right)^{-\frac{\nu t+2}{\nu}} \gamma\left(\frac{\nu t+2}{\nu}, \frac{(K+1)\phi}{\lambda_{RD_n}} R_n^{\nu}\right) \tag{B.2}$$

linear functions, and thus, it is a convex problem. Therefore, above problem can be solved by a convex method. The first-order derivative of (E.1) with $X_U$ and $Y_U$ can be computed as $2MX_U - 2\sum_{k=1}^{M} x_k$ and $2MY_U - 2\sum_{k=1}^{M} y_k$, respectively. When the first-order derivative equal to 0, the optimal solution can be obtain. Therefore, the optimal solutions of $X_U$ and $Y_U$ can be denoted as

$$X_U^* = \sum\nolimits_{k=1}^{M} x_k/M, \tag{E.2}$$

and

$$Y_U^* = \sum\nolimits_{k=1}^{M} y_k/M. \tag{E.3}$$

## REFERENCES

[1] E. G. Larsson, O. Edfors, F. Tufvesson, and T. L. Marzetta, "Massive MIMO for next generation wireless systems," IEEE Communications Magazine, vol. 52, no. 2, pp. 186–195, 2014.

[2] X. Li, X. Yang, L. Li, J. Jin, N. Zhao, and C. Zhang, "Performance analysis of distributed MIMO with ZF receivers over semi-correlated $\mathcal{K}$ fading channels," IEEE Access, vol. 5, pp. 9291–9303, 2017.

[3] K. Yang, N. Yang, N. Ye, M. Jia, Z. Gao, and R. Fan, "Non-orthogonal multiple access: Achieving sustainable future radio access," IEEE Communications Magazine, vol. 57, no. 2, pp. 116–121, February 2019.

[4] D. Wan, M. Wen, F. Ji, H. Yu, and F. Chen, "Non-orthogonal multiple access for cooperative communications: Challenges, opportunities, and trends," IEEE Wireless Communications, vol. 25, no. 2, pp. 109–117, April 2018.

[5] Z. Gao, L. Dai, D. Mi, Z. Wang, M. A. Imran, and M. Z. Shakir, "Mmwave massive-MIMO-based wireless backhaul for the 5G ultra-dense network," IEEE Wireless Communications, vol. 22, no. 5, pp. 13–21, October 2015.

[6] S. Alemaishat, O. Saraereh, I. Khan, S. Affes, and X. Li, "An efficient precoding scheme for millimeter-wave massive MIMO systems," Electronics, vol. 8, no. 9, p. 927, Aug 2019.

[7] C. Liu and L. Wang, "Optimal cell load and throughput in green small cell networks with generalized cell association," IEEE Journal on Selected Areas in Communications, vol. 34, no. 5, pp. 1058–1072, May 2016.

[8] X. Li, J. Li, L. Li, L. Du, J. Jin, and D. Zhang, "Performance analysis of cooperative small cell systems under correlated Rician/Gamma fading channels," IET Signal Processing, vol. 12, no. 1, pp. 64–73, 2018.

[9] M. Jia, X. Gu, Q. Guo, W. Xiang, and N. Zhang, "Broadband hybrid satellite-terrestrial communication systems based on cognitive radio toward 5G," IEEE Wireless Communications, vol. 23, no. 6, pp. 96–106, December 2016.

[10] X. Tang, K. An, K. Guo, Y. Huang, and S. Wang, "Outage analysis of non-orthogonal multiple access-based integrated satellite-terrestrial relay networks with hardware impairments," IEEE Access, vol. 7, pp. 141 258–141 267, 2019.

[11] T. Hou, Y. Liu, Z. Song, X. Sun, and Y. Chen, "Multiple antenna aided noma in UAV networks: A stochastic geometry approach," IEEE Transactions on Communications, vol. 67, no. 2, pp. 1031–1044, Feb 2019.

[12] J. Li, Y. Liu, X. Li, C. Shen, and Y. Chen, "Non-orthogonal multiple access in cooperative UAV networks: A stochastic geometry model," in 2019 IEEE 90th Vehicular Technology Conference (VTC2019-Fall), Sep. 2019, pp. 1–6.

[13] L. Zhang, H. Zhao, S. Hou, Z. Zhao, H. Xu, X. Wu, Q. Wu, and R. Zhang, "A survey on 5G millimeter wave communications for UAV-assisted wireless networks," IEEE Access, vol. 7, pp. 117 460–117 504, 2019.

[14] Z. Ding, Y. Liu, J. Choi, Q. Sun, M. Elkashlan, C. I, and H. V. Poor, "Application of non-orthogonal multiple access in LTE and 5G networks," IEEE Communications Magazine, vol. 55, no. 2, pp. 185–191, February 2017.

[15] X. Li, J. Li, Y. Liu, Z. Ding, and A. Nallanathan, "Residual transceiver hardware impairments on cooperative NOMA networks," IEEE Transactions on Wireless Communications, pp. 1–1, 2019.

[16] Z. Ding, Z. Yang, P. Fan, and H. V. Poor, "On the performance of non-orthogonal multiple access in 5G systems with randomly deployed users," IEEE Signal Processing Letters, vol. 21, no. 12, pp. 1501–1505, Dec 2014.

[17] S. Shi, L. Yang, and H. Zhu, "Outage balancing in downlink nonorthogonal multiple access with statistical channel state information," IEEE Transactions on Wireless Communications, vol. 15, no. 7, pp. 4718–4731, July 2016.

[18] X. Li, M. Zhao, W. U. Wu, J. Wu, K. M. Rabie, and R. Kharel, "Security analysis of multi-antenna NOMA networks under I/Q imbalance," Electronics, vol. 8, no. 1327, pp. 1–17, November 2019.

[19] Z. Ding, M. Peng, and H. V. Poor, "Cooperative non-orthogonal multiple access in 5G systems," IEEE Communications Letters, vol. 19, no. 8, pp. 1462–1465, Aug 2015.

[20] J. Kim and I. Lee, "Non-orthogonal multiple access in coordinated direct and relay transmission," IEEE Communications Letters, vol. 19, no. 11, pp. 2037–2040, Nov 2015.

[21] X. Li, M. Liu, C. Deng, P. T. Mathiopoulos, Z. Ding, and Y. Liu, "Full-duplex cooperative NOMA relaying systems with I/Q imbalance and imperfect SIC," IEEE Wireless Communications Letters, pp. 1–1, 2019.

[22] S. Lee, D. B. da Costa, Q. Vien, T. Q. Duong, and R. T. de Sousa, "Non-orthogonal multiple access schemes with partial relay selection," IET Communications, vol. 11, no. 6, pp. 846–854, 2017.

[23] X. Li, J. Li, and L. Li, "Performance analysis of impaired SWIPT NOMA relaying networks over imperfect weibull channels," IEEE Systems Journal, pp. 1–4, 2019.

[24] D. T. Do, A. T. Le, and B. M. Lee, "On performance analysis of underlay cognitive radio-aware hybrid OMA/NOMA networks with imperfect CSI," Electronics, vol. 8, no. 7, p. 819, 2019.
[25] X. Li, M. Liu, C. Deng, D. Zhang, X. Gao, K. M. Rabie, and R. Kharel, "Joint effects of residual hardware impairments and channel estimation errors on SWIPT assisted cooperative NOMA networks," IEEE Access, vol. 7, pp. 135 499–135 513, 2019.
[26] T. Shen and H. Ochiai, "A UAV-aided data collection for wireless powered sensor network over Rician fading channels," in 2019 16th IEEE Annual Consumer Communications Networking Conference (CCNC), Jan 2019, pp. 1–5.
[27] I. S. Gradshteyn and I. M. Ryzhik, Table of integrals, series, and products. Academic press, 2014.
[28] Alouini and Mohamed-Slim, Digital communication over fading channels, 2000.
[29] I. A. S. Abramowitz, Milton and R. H. Romer., Handbook of mathematical functions with formulas, graphs, and mathematical tables. Dover, 1970.
[30] A. Gil, J. Segura, and N. M. Temme, "Algorithm 939: Computation of the Marcum Q-function," ACM Transactions on MathComputer Software, vol. 40, pp. 280–295, 2014.
[31] E. Biglieri, R. Calderbank, A. Constantinides, A. Goldsmith, A. Paulraj, and P. HV, MIMO wireless communications, 2006.
[32] A. Goldsmith, Wireless Communications, 1st ed. Cambridge University Press, 2004.